Thermal Modeling of Five-Phase PMSG

5.1 Introduction

The electromagnetic design aspects of Single Stator Five Phase PMSG (SSFP-PMSG) and Novel Magnetically Coupled Dual Stator Five Phase PMSG (MCDSFP-PMSG) are covered in the last two Chapters 3 and 4. In this Chapter, thermal analyses of the developed generator have been reported.

This Chapter deals with the thermal modeling of both the proposed PMSGs. The lumped parameter model, FEM model and the temperature distribution of SSFP-PMSG are discussed in Section 5.2. The advanced lumped parameter model, FEM model and the temperature distribution of MCDSFP-PMSG are discussed in Section 5.3. The chapter is concluded in Section 5.4.

5.2 Thermal Circuit Model for SSFP-PMSG

Fig. 5.1 shows the schematic model of 60 slots, 8 pole, five-phase PMSG. It consists of stator and surface mounted permanent magnet rotor. Stator core is made up of thin laminations of high grade silicon steel alloy, these laminations are insulated from each other with high thermal resistant paper or varnish. The stator core houses the five phase double layer fractional slot short-pitched winding with 72^{o}E phase difference between adjacent phases. It consists of 240 turns in 12 coils per phase which is shown in Fig. 5.2. Coils are short-pitched by 12^{o}E that eliminates the higher order harmonic in the generated voltage and also reduces conductor copper loss and effective weight of the machine. The colours of different phases are red, green, blue, yellow and black for A, B, C, D and E phases respectively. This winding arrangement suppresses the higher order harmonics and reduces the copper requirement. The 8 permanent magnets are

mounted on the rotor surface. The 8 poles of rotor are confirmed by 8 flux loops which are shown in Fig. 5.3. The rating and corresponding dimensions of the designed generator is listed in Table 2.7.

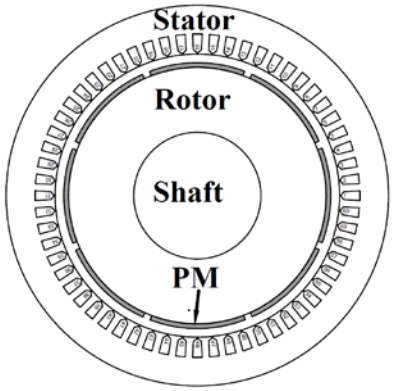

Fig. 5.1 Schematic of single stator single rotor Generator

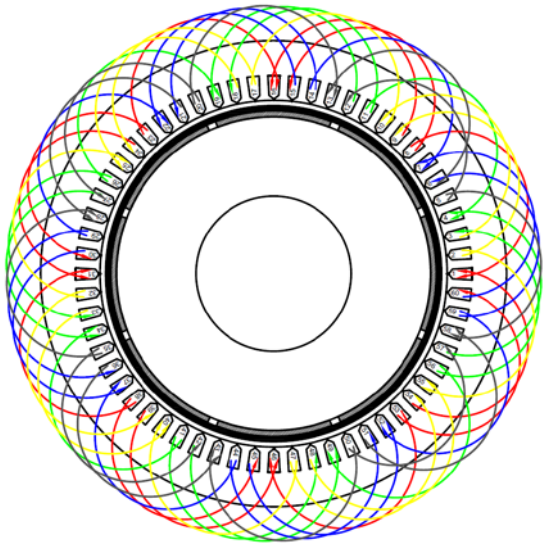

Fig. 5.2 Winding Pattern of SSFP-PMSG

5.2.1 Lumped Parameter Thermal Model

The lumped parameter thermal network of SSFF-PMSG is shown in Fig. 5.4. There are 8 nodes in the thermal network and the thermal resistances are connected between these nodes. In addition to the thermal capacitance, heat flow effect and heat

generation sources are also included in the model. Depending on the heat transfer mode the thermal resistances are divided into three categories namely conduction, convection and radiation. However radiation is not considered in the model, because it has very less effect for low rated machines.

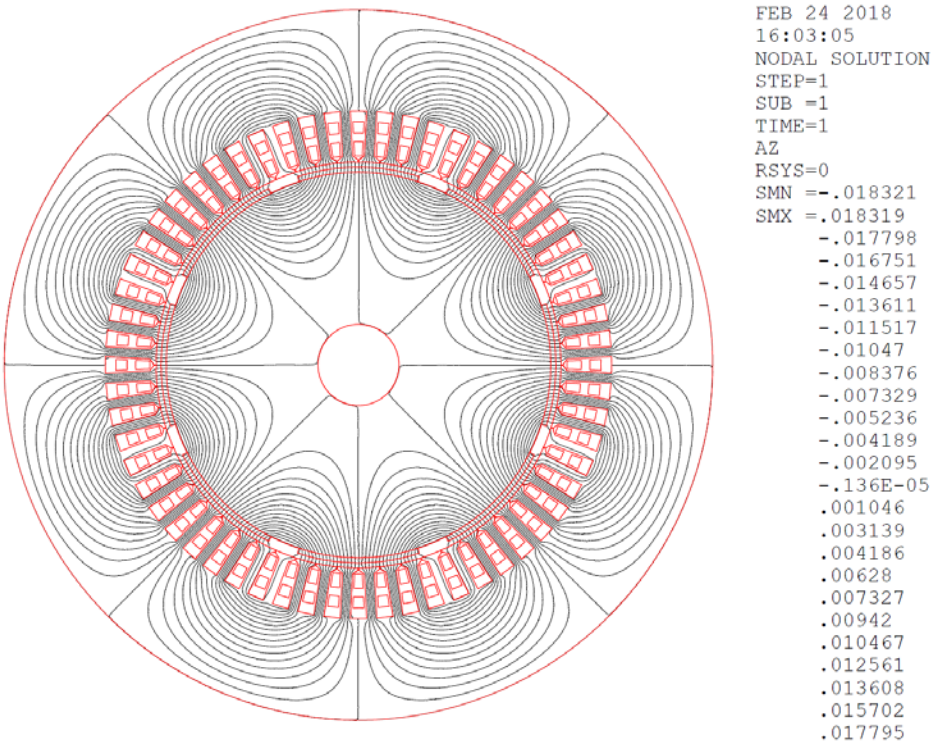

Fig. 5.3 Flux lines of eight poles of SSFP-PMSG

The following assumptions are taken during thermal modeling [151,152]:

1. Materials are anisotropic in nature.

2. The heat generation and thermal capacity are uniformly distributed in the model

3. The heat flow in axial and radial direction is independent of each-other.

4. The circumferential heat flow in the model is absent.

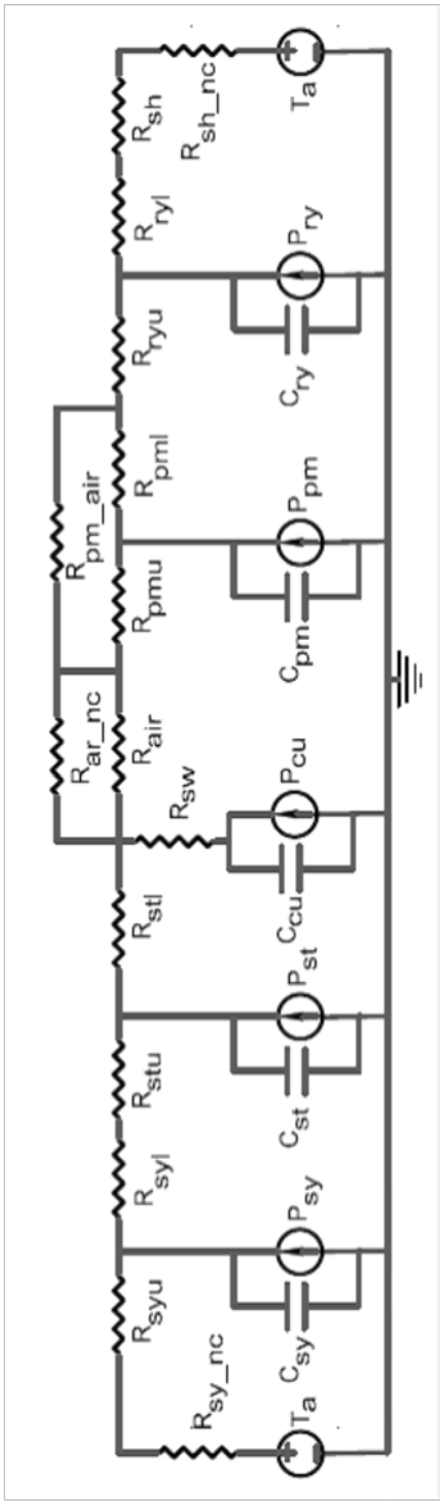

Fig. 5.4 Lumped Parameter Model

5.2.1.1 Thermal Conductive Resistance and Thermal Capacitance

For the steady state thermal analysis the thermal equilibrium equation can be written as follows.

$$[G][T]=[P] \tag{5.1}$$

where [G] is the thermal conductance matrix of the generator, [T] is the temperature rise of different nodes in the model and [P] is the loss matrix of the generator.

The general expression for the thermal conductive resistance between the nodes i and j:

$$R_{i,j}=\frac{l}{kA} \tag{5.2}$$

where l is the path length of conductive media, A is the area of cross-section and k is the thermal conductivity of material.

Most of the components like stator, rotor, PM and airgap of the generators are hollow cylinders as shown in figure 5.5. The T-type thermal network is used here for the development of lumped parameter model [150], [152]. The T-type network has four conductive thermal resistances, two for radial direction namely upper (R_u) and lower (R_l) corresponding to the mid-point and two for axial direction namely left (R_L) and right (R_R) side along the axial length corresponding to mid-point. The thermal capacitance (C) and power loss (P) corresponds to the components that are parallely connected. For simplicity, except shaft only radial direction heat flow is considered for SSFP-PMSG thermal model. The expressions for the thermal resistances of T-type network are as follow

Thermal conductive resistance (R_u)

$$R_u=\frac{l}{2\pi kL}\ln\frac{r_o}{r_m} \tag{5.3}$$

Where, k is the thermal conductivity, L is the axial length, r_o and r_m are the radius of outer surface and mid-point from the centre of the hollow cylindered.

Thermal conductive thermal resistance (R_l)

$$R_l = \frac{1}{2\pi kL} \ln \frac{r_m}{r_l} \tag{5.4}$$

where r_l is the radius of inner surface of the hollow cylindered.

Thermal conductive thermal resistance (R_L)

$$R_L = \frac{L}{2\pi kL\left(r_o^2 - r_i^2\right)} \tag{5.5}$$

Thermal conductive thermal resistance (R_R)

$$R_R = \frac{L}{2\pi kL\left(r_o^2 - r_i^2\right)} \tag{5.6}$$

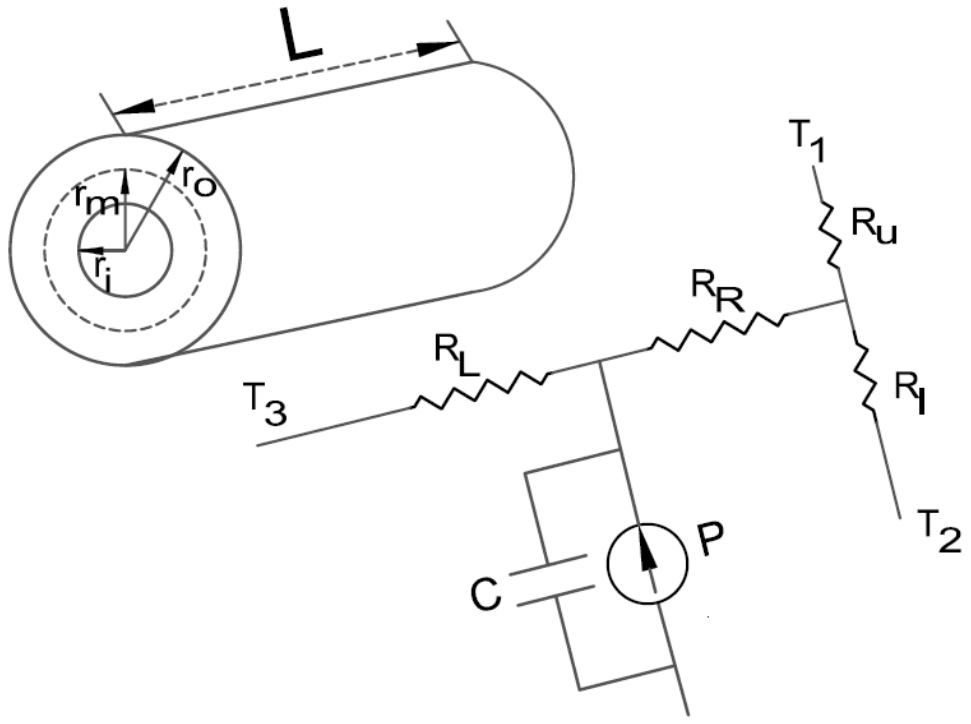

Fig. 5.5 Equivalent Thermal Lumped Parameter Model for a hollow cylinder

Thermal capacitance(C) can be expressed as

$$C = \rho V c_p \tag{5.7}$$

Where, cp is the specific heat, ρ is the material density and V is the volume of cylindrical region.

Table 5.1: Details of Material thermal properties [153]

Material	Specific heat (J/Kg^oC)	Density(Kg/m^3)	Thermal conductivity (W/m^oC)	Electrical resistivity (Ωm)
Iron	490	7650	44.2	$5*10^{-7}$
Copper	380	8993	401	$1.72*10^{-8}$
Permanent Magnet	420	7400	8.95	$160*10^{-8}$
Air	1007	1.13	0.02652	$1.93*10^{16}$
Insulation and wedge	940	1200	0.15	$5*10^{24}$

5.2.1.2 Equivalent Thermal Resistivity between Stator Slot Winding and Core

The Thermal resistivity between stator core and winding are different at different sides of slot, this is due to insulating layer and dimensional variation. The stator slots consists of impregnated copper conductor, wedge, paper insulation of slot liner, and insulating material between the two layers of winding, therefore the thermal conductivity between stator core to winding is not easy to define. Reference [154] suggests the possible approach to compute the thermal resistance as well as the equivalent thermal conductivity of winding impregnation and slot insulation.

The equivalent thermal conductivity (k_{eq}) can be expressed as

$$k_{eq} = \frac{\sum_{i=1}^{n} t_i}{\sum_{i=1}^{n} \frac{t_i}{k_i}} \tag{5.8}$$

where t_i is the thickness of different insulating layer and k_i is their respective thermal conductivity for the insulating material.

The equivalent thermal resistance between the winding and stator core are different in different parts because of dimensional variation.

The conductive thermal resistance between winding and stator core is calculated as

$$R_{wc} = \frac{t_{wc}}{k_{eq} A_{wc}} \tag{5.9}$$

where t_{wc} is the insulation thickness in the heat flow direction, A_{wc} is the cross-section area of contact between the insulation and core.

5.2.1.3 Thermal Convective Resistance

Convection is due to the variation of air density at the convective surface. Two types of convection are possible from the surface namely natural convection and forced convection. For the natural cooled machine, the outer stator to environment interface surface and the axial shaft to environment interface surface have natural convection, whereas the stator teeth to rotor interface surface can be natural or forced convection depending on the laminar and turbulent flow of heat.

The Convective thermal resistance can be expressed as

$$R = \frac{1}{h_c A} \tag{5.10}$$

where h_c is the convective heat transfer coefficient and A is the area of convective surface.

$$h_c = \frac{N_u \, k_{air}}{\delta} \tag{5.11}$$

N_{uh} is the Nusselt number and K_{air} is the thermal conductivity of air and δ is the characteristic length. The empirical formula for Nusselt number varies and depends on the natural and forced convection of heat from the surface [155].

For natural convection the Nusselt number (N_{uc}) is

$$N_{uc} = a\left(G_r \, P_r\right)^b \tag{5.12}$$

For force convection the Nusselt number (Nuf) is

$$N_{uf} = a \, R_e^b \, P_r^c \tag{5.13}$$

Where a, b and c are the constant, G_r is the Grashof number, P_r is the Prandtl number and R_e is the Reynolds number.

The empirical equations of Nusselt number used for the outer stator to environment interface surface N_{uh} and the axial shaft to environment interface surface N_{uv} are expressed as

$$N_{uh} = \left(0.6 + 0.387 \, R_a^{0.166}\left(1 + 0.721 \, P_r^{-0.5625}\right)^{-0.296}\right)^2 \tag{5.14}$$

$$N_{uv} = \left(0.825 + 0.387 \, R_a^{0.166}\left(1 + 0.671 \, P_r^{-0.5625}\right)^{-0.296}\right)^2 \tag{5.15}$$

$$R_a = G_r P_r = \frac{g\beta\left(T_s - T_\infty\right)\delta^3}{\upsilon^2} P_r \tag{5.16}$$

$$P_r = \frac{c_p \, \mu}{k_{air}} \tag{5.17}$$

Where R_a is the Rauleigh number, ν is the kinematic viscosity of air, g is the acceleration of gravity (m/sec^2), β is the coefficient of cubic expansion, T_s is the surface

temperature (^oC), T_∞ is the temperature (^oC) of air, δ is the characteristic length , c_p is the specific heat capacity at constant pressure (kJ/kg.^oC).

The Nusselt number used for the stator teeth to rotating rotor interface surface is decided by the Reynolds number and it depends on the speed of rotor. If the Reynolds number is less than the critical value (10^5) then the convective heat flow is laminar otherwise it is turbulent.

The Reynolds number (Re) is calculated as

$$R_e = \frac{\pi \rho_{air} N_r (\delta)^2}{60 \mu} \tag{5.18}$$

Where N_r is the rotor speed (RPM), ρ_{air} is the air density (Kg/m^3), μ is the dynamic viscosity (Kg/sec.m) of air. The calculated value of Reynolds number in this paper is $4.67x10^4$, which is less than the critical value of Reynolds number. The heat flow is therefore laminar and comes under natural convection.

The empirical formula of Nusselt number used for the stator teeth to rotor interface surface N_{uLa}.

$$N_{uLa} = \frac{0.886 R_e^{1/2} P_r^{1/2}}{\left(1 + \left(\frac{P_r}{0.0207}\right)^{2/3}\right)^{1/4}} \tag{5.19}$$

Using equation (5.10), (5.11) and (5.15) the convective heat transfer coefficient for the outer stator to environment interface surface, axial shaft to environment interface surface and the stator teeth to rotating rotor interface surface are 23.4014, 4.9263 and 958.3188 (w/m^2.K) respectively.

For calculating the thermal model lumped parameters of different parts of machine Eqn. (5.2), Eqn. (5.3), Eqn. (5.4), Eqn. (5.7), Eqn. (5.9) and Eqn. (5.10) have been used. It required dimensional details and the material properties which are listed in Table 2.7

and Table 5.1 respectively. The calculated thermal parameters for the SSFP-PMSG are listed in Table 5.2.

Table 5.2: List of thermal Parameters of SSFP-PMSG

Thermal Parameter	Value	Unit
R_{sh_nc}	243.6461	Kelvin (K) per watt (W)
R_{sh}	0.4276	K/W
R_{ryl}	0.0400	K/W
R_{ryu}	0.0190	K/W
R_{pml}	0.0031	K/W
R_{pmu}	0.0030	K/W
R_{pm_air}	8.2046	K/W
R_{air}	1.5994	K/W
R_{ar_nc}	11.0571	K/W
R_{sw}	0.4630	K/W
R_{stl}	0.0087	K/W
R_{stu}	0.0087	K/W
R_{syl}	0.0075	K/W
R_{syu}	0.0062	K/W
R_{sy_nc}	5.3990	K/W
C_{ry}	9649.2	Joule (J) per Kelvin (K)
C_{pm}	361.5754	J/K
C_{cu}	1201.2	J/K
C_{st}	2256.3	J/K
C_{sy}	16906	J/K

5.2.1.4 Loss Calculation in Different Parts of Model

Core loss in the stator yoke, stator tooth and rotor yoke has been calculated as follows:

1. Stator core loss

Iron loss in stator yoke is expressed as:

$$P_{sy}=k_e f^2 B_{sy}^2+k_h f B_{sy}^2+k_a f^{1.5} B_{sy}^{1.5} \quad (5.20)$$

Iron loss in stator tooth is expressed as:

$$P_{st}=k_e f^2 B_{st}^2+k_h f B_{st}^2+k_a f^{1.5} B_{st}^{1.5} \quad (5.21)$$

Where k_e is the coefficient of eddy current constant, k_h is the coefficient of hysteresis constant, k_a is the coefficient of excess loss constant, B_{sy} is the peak flux density in the iron core, B_{st} is the peak flux density in the stator tooth and f is the frequency (Hz).

2. Copper loss of stator winding

The copper loss is the prime contributor to loss in PM machine, it is due the resistivity of copper wire in the per phase winding.

The total copper loss in the winding is expressed as:

$$P_{cu}=\sum_{m=1}^{5} I^2 R_{ph} \quad (5.22)$$

Where I is the phase current R_{ph} is the phase resistance and *m* is the number of phases.

3. Rotor loss

The rotor loss is divided into two parts namely core loss and permanent magnet loss. The rotor core loss is due to the eddy current loss, hysteresis loss and excess loss in the rotor whereas the permanent magnet loss is due to the eddy current developed in it. The rotor core loss can be calculated by the following formula

$$P_{ry} = k_e f^2 B_{ry}^2 + k_h f B_{ry}^2 + k_a f^{1.5} B_{ry}^{1.5} \quad (5.23)$$

Where B_{ry} is the peak flux density in the rotor core.

The procedure and the expression developed for eddy current loss for permanent magnet is mentioned in [156] and [157]. The conductivity for the NdFeB is $7.7x10^5$ s/m.

Permanent magnet loss is calculated as

$$P_{pm} = w_e^2 \left(\sum_{k=1}^{\infty} B_g^2 \right) \frac{N_a N_c V_{pm} m_o^3}{16 \rho_{pm} \left(C_{eff} + m_o^2 \right)} \frac{\frac{W_{pm}}{N_c}}{\frac{L_{pm} N_c}{W_{pm} N_a}} \left(\begin{array}{l} \frac{1}{2} + \frac{2}{3} \frac{\left(2C_{eff} + m_o^2 \right) \left(\frac{L_{pm} N_c}{W_{pm} N_a} - m_o \right)}{m_o \left(C_{eff} + m_o^2 \right)} + \frac{C_{eff}^2 \left(\frac{L_{pm} N_c}{W_{pm} N_a} - m_o \right)^2}{m_o^2 \left(C_{eff} + m_o^2 \right)} - \\ \frac{2C_{eff}^2 \left(\frac{L_{pm} N_c}{W_{pm} N_a} - m_o \right)^3}{m_o \left(C_{eff} + m_o^2 \right)^3} + \frac{2C_{eff}^2 \left(\frac{L_{pm} N_c}{W_{pm} N_a} - m_o \right)^4}{\left(C_{eff} + m_o^2 \right)^4} \ln \left(1 + \frac{C_{eff} + m_o^2}{m_o \left(\frac{L_{pm} N_c}{W_{pm} N_a} - m_o \right)} \right) \end{array} \right) \quad (5.24)$$

where w_e is the electrical angular speed (rad/sec), B_g is the flux density, N_a is the number of axial segment, N_c is the number of arcillier segment, V_{pm} is the volume of magnet, ρ_{pm} is the resistivity of magnet, m_o is the slope of line passing through the path of eddy current edge, C_{eff} (≥ 1) is the factor of incremental path length of eddy current, L_{pm} is the length of permanent magnet and W_{pm} is the width of permanent magnet.

5.2.2 Finite Element Method

The finite element model analysis has been done using ANSYS software. This method requires a fast processor with a large storage device and takes around two hours for simulation but it is highly accurate. In this paper, there are two solver used for the thermal analysis namely harmonic analysis and transient analysis. These analyses are performed by setting element type (quad 4, node 13), degree of freedom, material properties and meshing the model into 227720 elements. The harmonic analysis uses AZ degree of freedom for the elements when calculating the losses and heat generation

rate in different parts of the model. The heat generation rate which is stored in .rmg file from this analysis is further used for the thermal analysis. The elemental degree of freedom Temp is used for the thermal analysis. The analysis type (transient), time at the end of load step (86400 sec), load heat generation from MAG Analysis, boundary condition (Convection), are taken in solution step. The results of Temperature distribution, radial temperature distribution and heat flux plot are shown in postprocessor steps.

Fig. 5.6 shows the temperature distribution in the model and it is found that the winding temperature is highest whereas the shaft temperature is least. Since machine is naturally cooled so the heat is released to the environment via outer stator surface and the shaft. Although, the convective area of the shaft is less than the outer stator, but the shaft temperature 113.869^{o} C is less than the outer stator yoke temperature 119.231^{o} C this is because of conduction of heat from winding to outer stator yoke is higher.

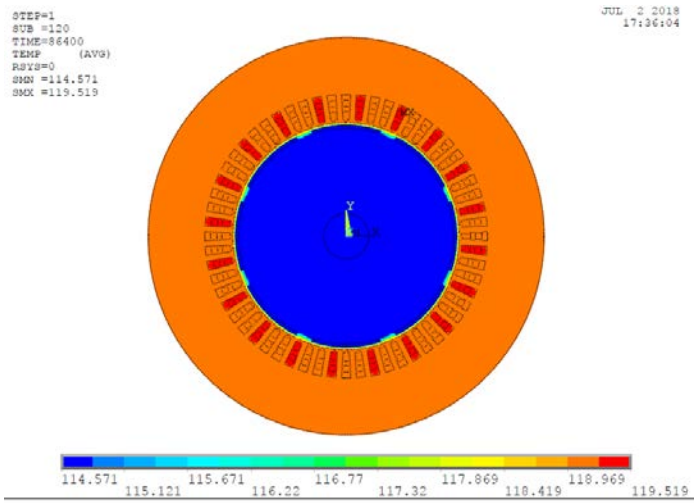

Fig. 5.6 Temperature distribution in the model

Fig. 5.7 shows the temperature rise in different parts of the model. The FEM simulation runs for 24 hours and the steady state temperature is attained by the model in around 16 hours.

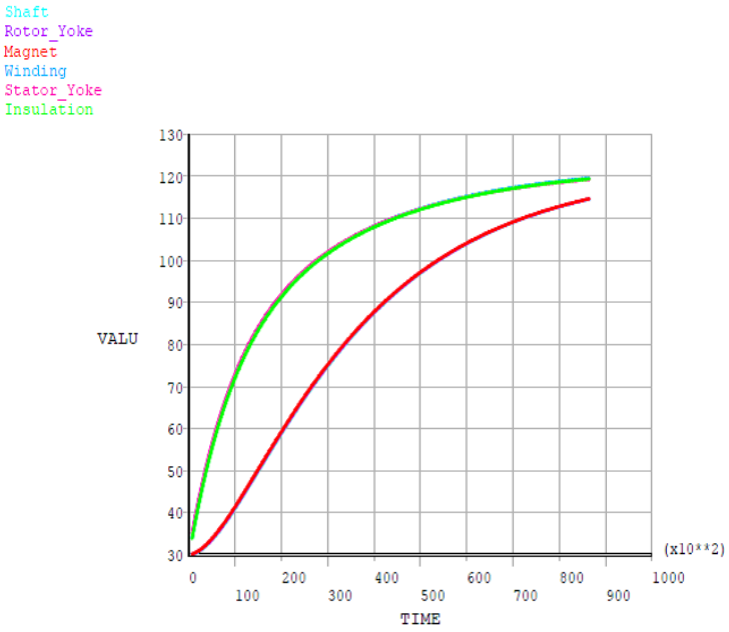

Fig. 5.7 Temperature developed in the model

The radial temperature distribution is shown in Fig. 5.8. The temperatures of the shaft and rotor yokes are found at the same level because of heat transfer in conduction mode. A sharp increment is found at winding and it decreases at the stator yoke surface due to convection process to environment.

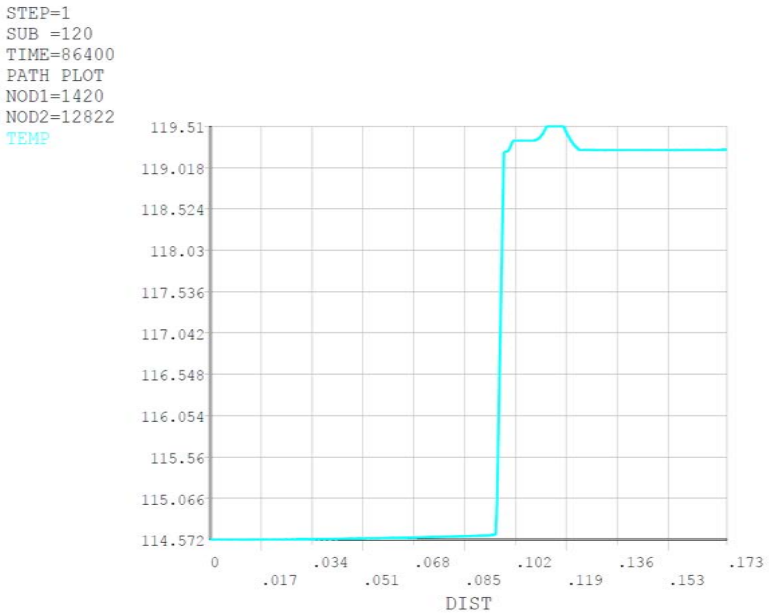

Fig. 5.8 Radial temperature distribution

5.2.3 Validation of Predicted Results using Lumped Parameter Model

The predicted temperature using the lumped parameter method for shaft is shown in Fig. 5.9. It is observed that the settling time to attain steady state temperature is comparatively lower for Lumped Parameter Model [LPM] than FEM. The estimated steady state temperature of the shaft is 113.869ºC. The shaft temperature effects the bearing lubrication and could lead towards reduced viscosity or increased friction. This affect requires regular monitoring and maintenance else deteriorated bearings could eventually result in eccentricity fault of the machine.

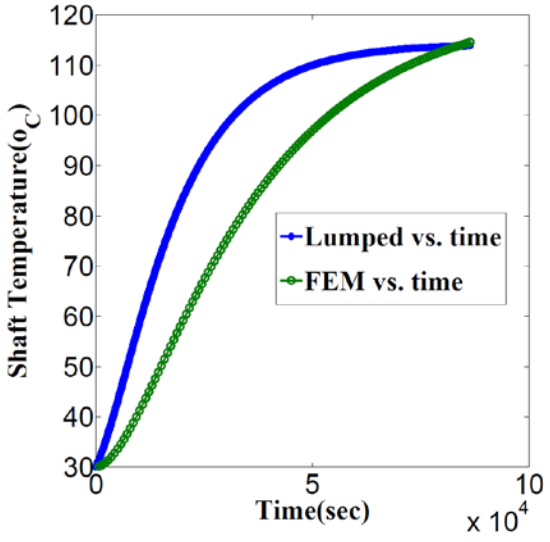

Fig. 5.9 Shaft temperature

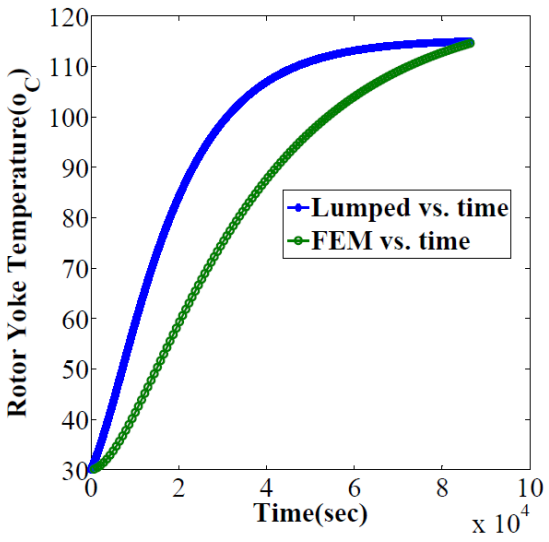

Fig. 5.10 Rotor Yoke temperature

Fig. 5.10 shows that the steady state temperature of the rotor yoke is 114.997ºC. Lamination of the rotor yoke is required to reduce the eddy current losses. For this a thin layer of insulation is placed between the cores. Table 2.3 lists the insulation materials for lamination and corresponding maximum operating temperature. The Class B insulating material is therefore appropriate for rotor yoke lamination.

The permanent magnet temperature is shown in Fig. 5.11. For the NdFeB magnets the steady state temperature is 115.15ºC.

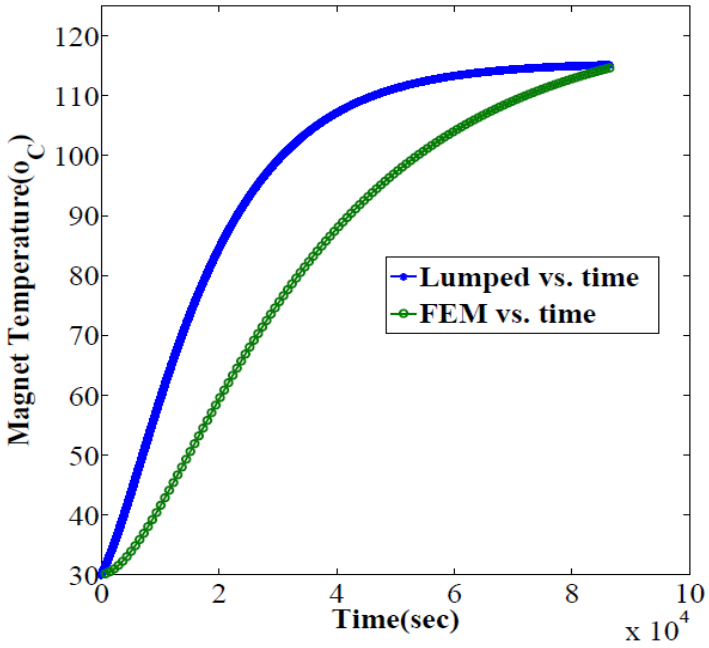

Fig. 5.11 Magnet temperature

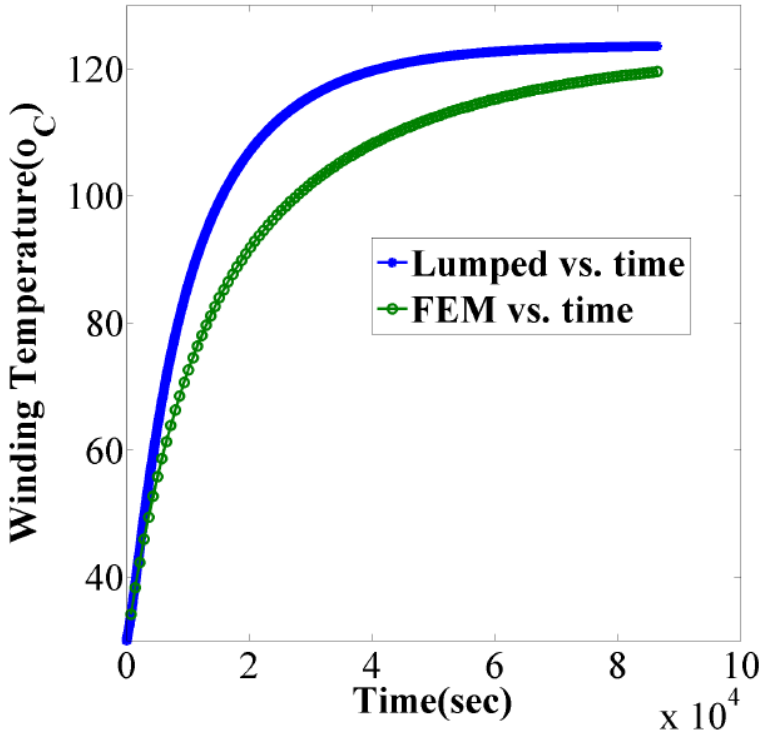

Fig. 5.12 Winding temperature

Different grade of NdFeB permanent magnets is shown in Table 2.6. For the proposed SSFP-PMSGthe NdFeB H grade magnet seems appropriate.

The maximum temperature of the SSFP-PMSG appears at the winding. For the proposed machine the steady state winding temperature is 123.528ºC as shown in Fig. 5.12. Appropriate winding insulation is mandatory to ensure safe operation of the machine.

The list of winding insulating materials is shown in Table 2.1. The class B winding insulating material is the optimum material for this purpose.

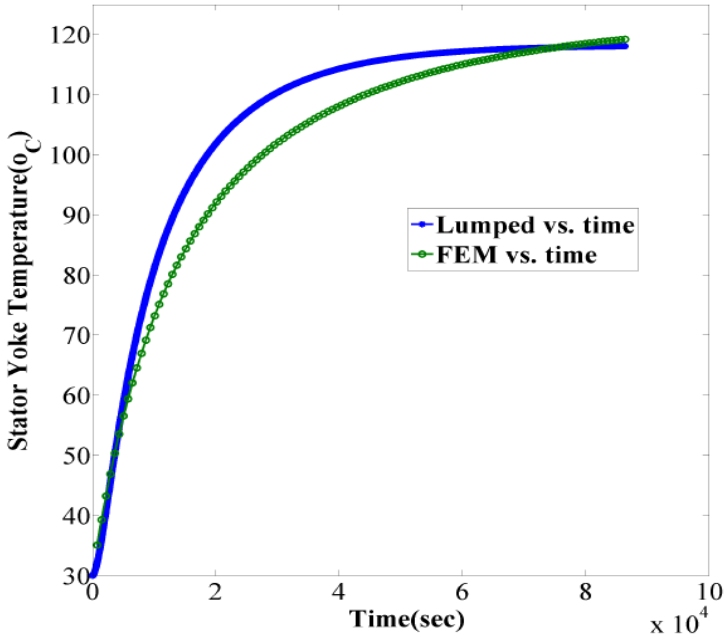

Fig. 5.13 Stator Yoke temperature

The temperature build up process in the stator yoke is shown in Fig. 5.13. From this figure the steady state temperature of the stator yoke is 118.063ºC. Using Table 2.3, the Class B insulating material is the appropriate choice for stator yoke laminations.

In a comprehensive manner the estimated temperature of the various sections of the proposed SSFP-PMSG using LPM and FEM is presented in Table 5.3. The percentage of error between the predicted temperature results using LPM and FEM results are very close. This confirms the capability of Lumped parameter model in analysing quick and reasonably accurate results for the proposed SSFP-PMSG.

Table 5.3: Steady state temperature of different part of SSFP-PMSG

Parameter	Lumped (in ^{O}C)	FEM (in ^{O}C)	%Error
Shaft	113.869	114.572	-0.617
Rotor Yoke	114.997	114.597	0.347
Magnet	115.151	114.632	0.45
Winding	123.528	119.510	3.253
Stator Yoke	118.063	119.231	-0.989

5.2.4 Summary

The Section 5.2 deals with the thermal modelling for the SSFP-PMSG. For the thermal modelling lumped parameter method is used, which is simple and fast technique for predicting the temperature distribution inside the proposed generator. As the permanent magnet is the most sensitive part of the machine so losses in it are discussed in detail. Based on the predicted temperature various materials are identified for the development and safe operation of the machine. Maintenance issues due to shaft temperature on bearing lubrication viscosity are also highlighted. The error between the predicted and FEM are found within 4% limit which ensures the accuracy of predicted results using lumped parameter model for the proposed SSFP-PMSG.

Although, the accuracy of the presented lumped parameter is found appreciable it can be further improved by including the axial direction heat flow and heat radiation effects. By keeping points in view the Lumped parameter thermal model is for the MCDSFP-PMSG is developed, which is mentioned in the Section 5.3.

5.3 Thermal Circuit Model for MCDSFP-PMSG

The schematic of the MCDSFP-PMSG is presented in Fig 5.14. It consists of two stators and one segmented annular rotor. The outer stator consists of 60 slots where as

inner stator 20, which are occupied by the two sets of five phase 8 poles balanced double layer fractional slot windings. The outer stator winding consists of 432 turns in 12 coils per phase and inner stator winding consists of 112 turns in 4 coils which is shown in Fig. 5.15. The outer winding coils are short-pitched by 12^{o}E and the winding coils are short-pitched by 36^{o}E that eliminates the higher order harmonic in the generated voltage and also reduces conductor copper loss and effective weight of the machine. The two sets of 8 permanent magnets are placed on both the surfaces of eight segments of the rotor. Permanent magnets of same grades are arranged in such a way that the MMFs of both the magnets combine together and set-up a common flux in their air-gaps. The 8 poles of rotor are confirmed by 8 flux loops which are shown in Fig. 5.16. The specification and design details of the machine are given in Table 2.8.

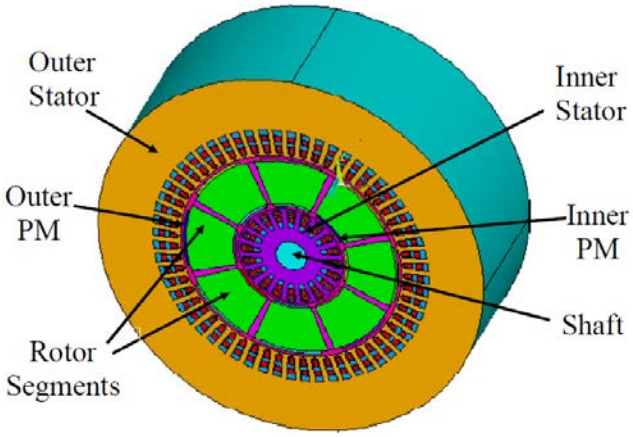

Fig. 5.14 Schematic of MCDSFP-PMSG

5.3.1 Lumped Parameter Thermal Model for MCDSFP-PMSG

Fig. 5.17 represents the lumped parameter of thermal model for MCDSFP-PMSG. The thermal resistances in this network are broadly divided as conductive, convective and radiation. Since the heat in each part of generator is flowing in both the radial and axial direction so conductive thermal resistance is divided as upper and lower in the radial direction and left and right in the axial direction. The convective and

radiation thermal resistances are connected in parallel for natural cooling. This cooling is from left and

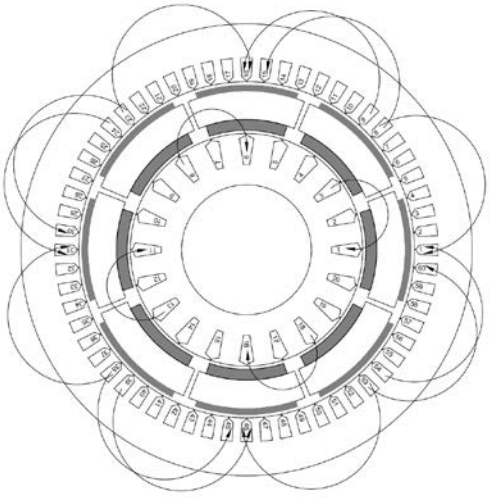

Fig. 5.15 Winding Layout of MCDSFP-PMSG

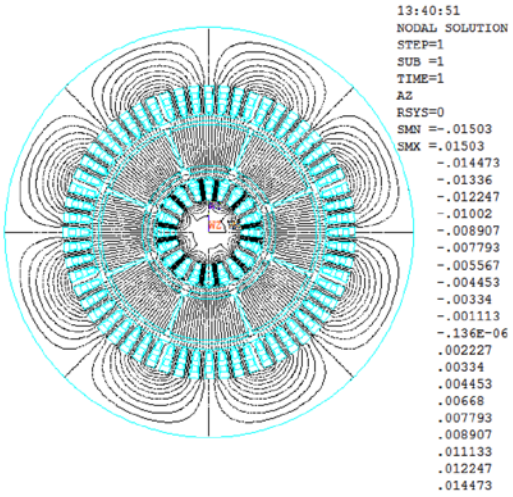

Fig. 5.16 Flux lines confirming Eight Poles of MCDSFP-PMSG

right sides in the axial direction as well as the outer surface of outer stator, inner and outer PM and shaft to the environment. The power loss like copper loss, core loss and eddy current loss are represented as equivalent current sources injected at appropriate nodes of the thermal network. The resulting node voltages represent their temperature.

The environment temperature has taken as ambient temperature which is constant at 30^{o}C. The assumptions are considered as mentioned in the Subsection 5.2.1.

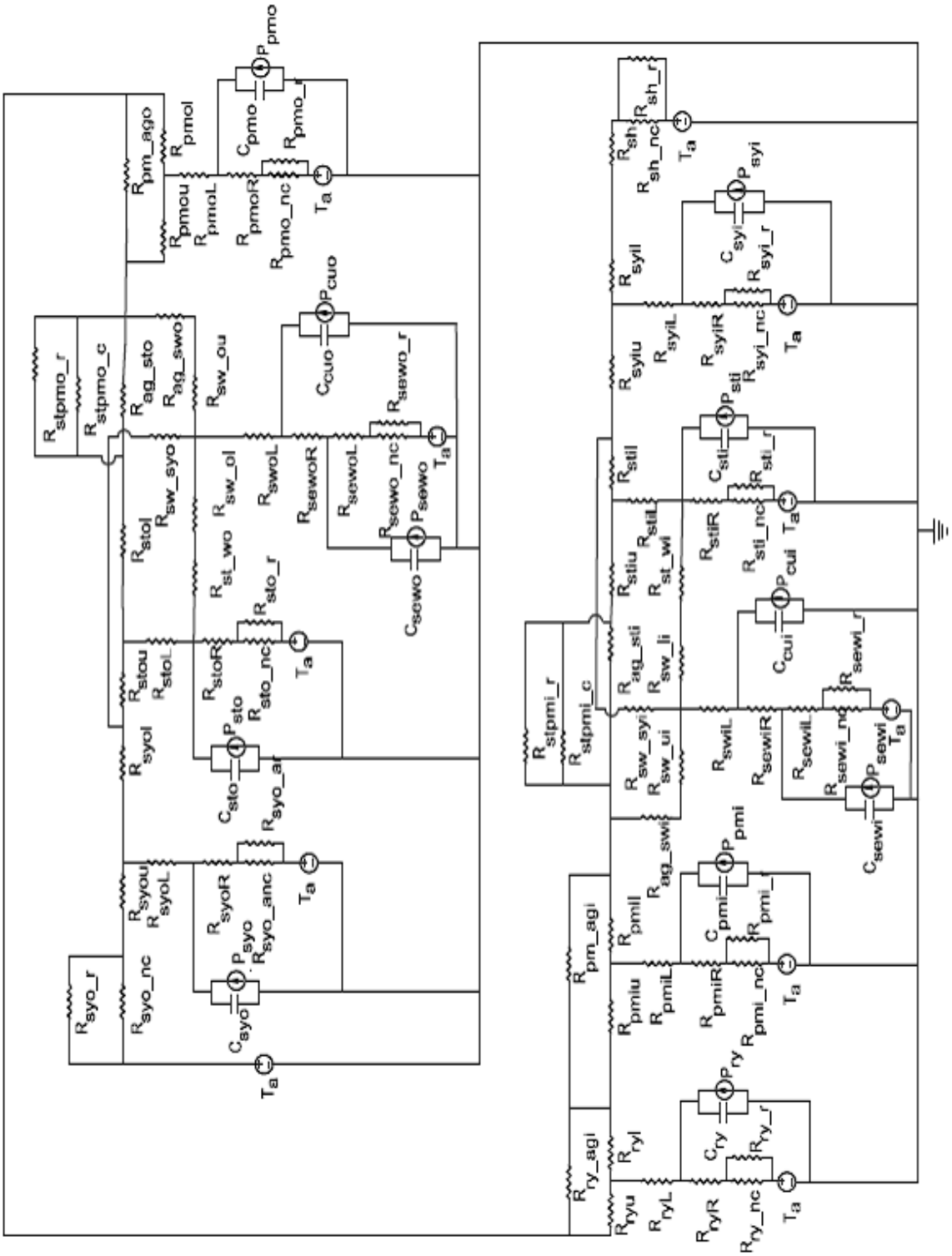

Fig. 5.17 Lumped parameter thermal model of MCDSFP-PMSG

5.3.1.1 Thermal Conductive Resistance and Thermal Capacitance

For thermal analysis, all the thermal parameters are calculated similarly as the SSFP-PMSG using the Eqn. (5.2) - Eqn. (5.7) as discussed in Subsection 5.2.1.1. For calculating the thermal model lumped parameters of different parts of machine, the required dimensional details and the material properties are used which are listed in Table 2.8 and Table 5.1 respectively. Since the lumped parameter thermal model of MCDSFP-PMSG also includes the radiation effect so the following are the main equations for calculating the radiation thermal parameter.

The power loss due to thermal radiation can be expressed as

$$P_{Rad} = \mathrm{e}\ \sigma\left(T_{s1}^4 - T_{s2}^4\right) \tag{5.25}$$

Where P_{Rad} is the power transferred per unit area, 'e' is the emissivity of the surface, 'σ' is the Stefan-Boltzmann constant which is $5.67\text{x}10^{-8}$ $W.m^{-2}.K^{-4}$ and T_{s1} and T_{s2} are the temperature of two surfaces in Kelvin.

The radiation thermal resistance can be expressed as

$$R_{Rad} = \frac{1}{\alpha_{Rad} A_s} \tag{5.26}$$

Whereas α_{Rad} is the coefficient of radiation and A_s is the surface area

$$\alpha_{Rad} = \frac{P_{Rad}}{\left(T_{s1} - T_{s2}\right)} \tag{5.27}$$

5.3.1.2 Equivalent Thermal Resistivity between Stator Slot Winding and Core

The thermal resistance between both the stator core and windings for MCDSFP-PMSG is found similarly as the method mentioned in Subsection 5.2.1.2 with the help of Eqn. (5.8) and Eqn. (5.9).

5.3.1.3 Thermal Convective Resistance

There are two types of convection process possible from the surface to air namely natural and forced convection. For the naturally cooled PMSG, the outer stator surface, left and right side of surface along the axial length and the axial shaft to environment interface surface have natural convection, whereas both the stator teeth to rotor interface surface can be natural or forced convection depending on the laminar and turbulent flow of heat. By using the Eqn. (5.10) - Eqn. (5.19) the convective thermal resistance of different parts are calculated.

The all the calculated thermal parameters of the lumped parameter model for MCDSFP-PMSG are listed in the Table 5.4.

Table 5.4: List of thermal Parameters of MCDSFP-PMSG

Thermal Parameter	Value	Unit
R_{sh}	1.1477	K/W
R_{sh_r}	285.2562	K/W
R_{sh_nc}	439.2531	K/W
R_{syil}	0.0118	K/W
R_{syiu}	0.0084	K/W
R_{syiL}	0.7508	K/W
R_{syiR}	0.7508	K/W
R_{syi_r}	93.2568	K/W
R_{syi_nc}	1104.7	K/W
R_{stil}	0.0172	K/W
R_{stiu}	0.0172	K/W
R_{stiL}	0.0012	K/W

R_{stiR}	0.0012	K/W
R_{sti_r}	0.2166	K/W
R_{sti_nc}	0.0090	K/W
R_{st_wi}	0.0585	K/W
R_{ag_sti}	2.4769	K/W
R_{stpmi_r}	3.4058	K/W
R_{stpmi_c}	11.8867	K/W
R_{ag_swi}	30.1659	K/W
R_{pm_agi}	11.7765	K/W
R_{ry_agi}	139.5397	K/W
R_{sw_syi}	0.0118	K/W
R_{sw_li}	0.1190	K/W
R_{sw_ui}	0.1190	K/W
R_{swiL}	2.435	K/W
R_{sewiL}	0.1129	K/W
R_{sewiR}	0.1129	K/W
R_{sewi_nc}	1717.7	K/W
R_{sewi_r}	114.4925	K/W
R_{pmil}	0.0044	K/W
R_{pmiu}	0.0043	K/W
R_{pmiL}	8.7220	K/W
R_{pmiR}	8.7220	K/W
R_{pmi_r}	252.5804	K/W
R_{pmi_nc}	4723.3	K/W

R_{ryl}	0.0099	K/W
R_{ryu}	0.0073	K/W
R_{ryL}	0.0714	K/W
R_{ryR}	0.0714	K/W
R_{ry_r}	0.0513	K/W
R_{ry_nc}	0.00095124	K/W
R_{pmol}	0.0023	K/W
R_{pmou}	0.0023	K/W
R_{pmoL}	4.6170	K/W
R_{pmoR}	4.6170	K/W
R_{pmo_r}	134.6582	K/W
R_{pmo_nc}	1793.5	K/W
R_{pm_ago}	6.2330	K/W
R_{ag_sto}	1.2150	K/W
R_{ag_swo}	30.16	K/W
R_{stpmo_c}	8.4194	K/W
R_{stpmo_r}	1.7908	K/W
R_{sw_syo}	0.0069	K/W
R_{sw_ol}	0.0309	K/W
R_{sw_ou}	0.0309	K/W
R_{swoL}	0.253	K/W
R_{sewoR}	0.0723	K/W
R_{sewoL}	0.0723	K/W
R_{sewo_nc}	878.1916	K/W

R_{sewo_r}	32.1372	K/W
R_{st_wo}	0.0185	K/W
R_{stol}	0.0060	K/W
R_{stou}	0.0060	K/W
R_{stoL}	0.00037707	K/W
R_{stoR}	0.00037707	K/W
R_{sto_nc}	0.0030	K/W
R_{sto_r}	0.0764	K/W
R_{syol}	0.0118	K/W
R_{syou}	0.0084	K/W
R_{syoL}	0.7508	K/W
R_{syoR}	0.7508	K/W
R_{syo_anc}	3.3167	K/W
R_{syo_ar}	3.5875	K/W
R_{syo_r}	1.3305	K/W
R_{syo_nc}	3.5082	K/W
C_{syi}	882.4558	J/K
C_{sti}	854.6688	J/K
C_{cui}	559.5006	J/K
C_{sewi}	265.3519	J/K
C_{pmi}	242.8125	J/K
C_{ry}	9277.8	J/K
C_{pmo}	437.0625	J/K
C_{cuo}	2158.1	J/K

C_{sewo}	2529.8	J/K
C_{sto}	2699.0	J/K
C_{syo}	882.4558	J/K

5.3.1.4 Loss Calculation in Different Parts of Model

The Core loss namely inner stator yoke, inner stator tooth, outer stator yoke, outer stator tooth and rotor yoke are calculated using equations Eqn. (5.20), Eqn. (5.21) and Eqn. (5.23). The copper loss in both the winding are calculated using Eqn. (5.22).

The inner permanent magnet loss is calculated as

$$P_{pm} = w_e^2\left(\sum_{k=1}^{\infty} B_{gi}^2\right)\frac{N_a N_c V_{pm} m_o^3}{16\rho_{pm}\left(C_{eff}+m_o^2\right)}\frac{\frac{W_{pm}}{N_c}}{\frac{L_{pm}N_c}{W_{pm}N_a}}\left(\begin{array}{l}\frac{1}{2}+\frac{2}{3}\frac{\left(2C_{eff}+m_o^2\right)\left(\frac{L_{pm}N_c}{W_{pm}N_a}-m_o\right)}{m_o\left(C_{eff}+m_o^2\right)}+\frac{C_{eff}^2\left(\frac{L_{pm}N_c}{W_{pm}N_a}-m_o\right)^2}{m_o^2\left(C_{eff}+m_o^2\right)}- \\ \frac{2C_{eff}^2\left(\frac{L_{pm}N_c}{W_{pm}N_a}-m_o\right)^3}{m_o\left(C_{eff}+m_o^2\right)^3}+\frac{2C_{eff}^2\left(\frac{L_{pm}N_c}{W_{pm}N_a}-m_o\right)^4}{\left(C_{eff}+m_o^2\right)^4}\ln\left(1+\frac{C_{eff}+m_o^2}{m_o\left(\frac{L_{pm}N_c}{W_{pm}N_a}-m_o\right)}\right)\end{array}\right) \quad (5.28)$$

The outer permanent magnet loss is calculated as

$$P_{pm} = w_e^2\left(\sum_{k=1}^{\infty} B_{go}^2\right)\frac{N_a N_c V_{pm} m_o^3}{16\rho_{pm}\left(C_{eff}+m_o^2\right)}\frac{\frac{W_{pm}}{N_c}}{\frac{L_{pm}N_c}{W_{pm}N_a}}\left(\begin{array}{l}\frac{1}{2}+\frac{2}{3}\frac{\left(2C_{eff}+m_o^2\right)\left(\frac{L_{pm}N_c}{W_{pm}N_a}-m_o\right)}{m_o\left(C_{eff}+m_o^2\right)}+\frac{C_{eff}^2\left(\frac{L_{pm}N_c}{W_{pm}N_a}-m_o\right)^2}{m_o^2\left(C_{eff}+m_o^2\right)}- \\ \frac{2C_{eff}^2\left(\frac{L_{pm}N_c}{W_{pm}N_a}-m_o\right)^3}{m_o\left(C_{eff}+m_o^2\right)^3}+\frac{2C_{eff}^2\left(\frac{L_{pm}N_c}{W_{pm}N_a}-m_o\right)^4}{\left(C_{eff}+m_o^2\right)^4}\ln\left(1+\frac{C_{eff}+m_o^2}{m_o\left(\frac{L_{pm}N_c}{W_{pm}N_a}-m_o\right)}\right)\end{array}\right) \quad (5.29)$$

where w_e is the electrical angular speed (rad/sec), B_{gi} and B_{go} are the flux densities of inner and outer air-gap, N_a is the number of axial segment, N_c is the number of Arcillier segment, V_{pm} is the volume of magnet, ρ_{pm} is the resistivity of magnet, m_o is the slope of

line passing through the path of eddy current edge, C_{eff} (≥1) is the factor of incremental path length of eddy current, L_{pm} is the length of permanent magnet and W_{pm} is the width of permanent magnet.

5.3.2 Finite Element Method

The thermal analysis using FEM of MCDSFP-PMSG has been done similarly as for the SSFP-PMSG mentioned in Section 5.2.2. Fig 5.18 presents the temperature distribution inside the model; it confirms that the inner stator region having higher temperature than the outer stator surfaces. Though shaft is also in contact with the environment but it's unable to cool sufficiently as it has smaller surface area. The outer stator surface area is larger, so the temperature of the inner stator is 24.39 % higher than the outer stator. In addition the magnet temperature of inner is 0.1166 % higher than outer magnet and the winding insulation of inner is 19 % higher than the outer stator winding. Fig. 5.19 provides a steady state as well as the transient state temperature variation at different nodal position in the model. The radial temperature distribution from shaft to outer stator surface is shown in Fig. 5.20.

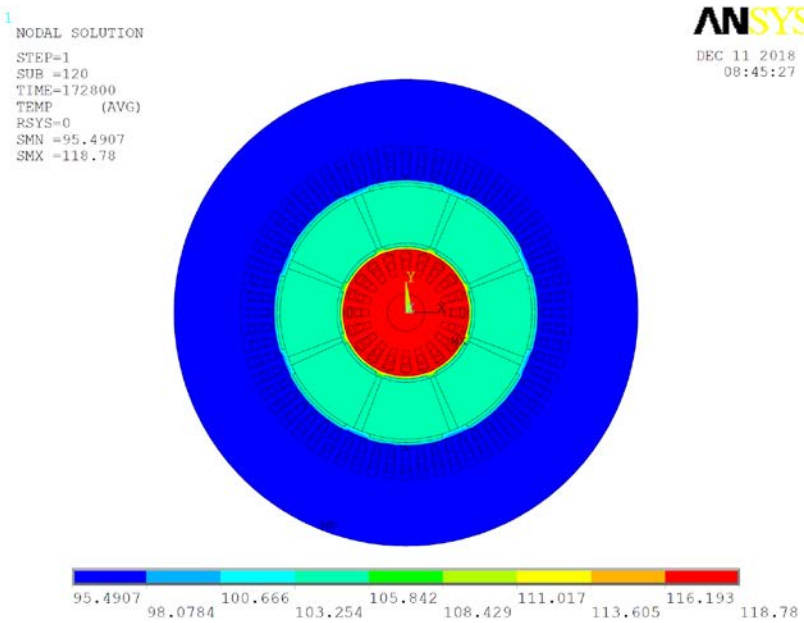

Fig. 5.18 Temperature distribution in the model

5.3.3 Validation of Predicted Results using Lumped Parameter Model

Fig. 5.21 shows the predicted and simulated temperature result for the shaft using the lumped parameter method and FEM. The error in steady state temperature using lumped parameter is 2.9 % higher than the FEM results. The predicted steady state temperature using lumped parameter model method is 114.764^{o}C which is higher than FEM result. The shaft temperature effects the bearing lubrication and reduces the viscosity which results in increased friction. This affect arises the necessity of frequent monitoring and maintenance, else deteriorated bearings could eventually result in eccentricity fault of the generator.

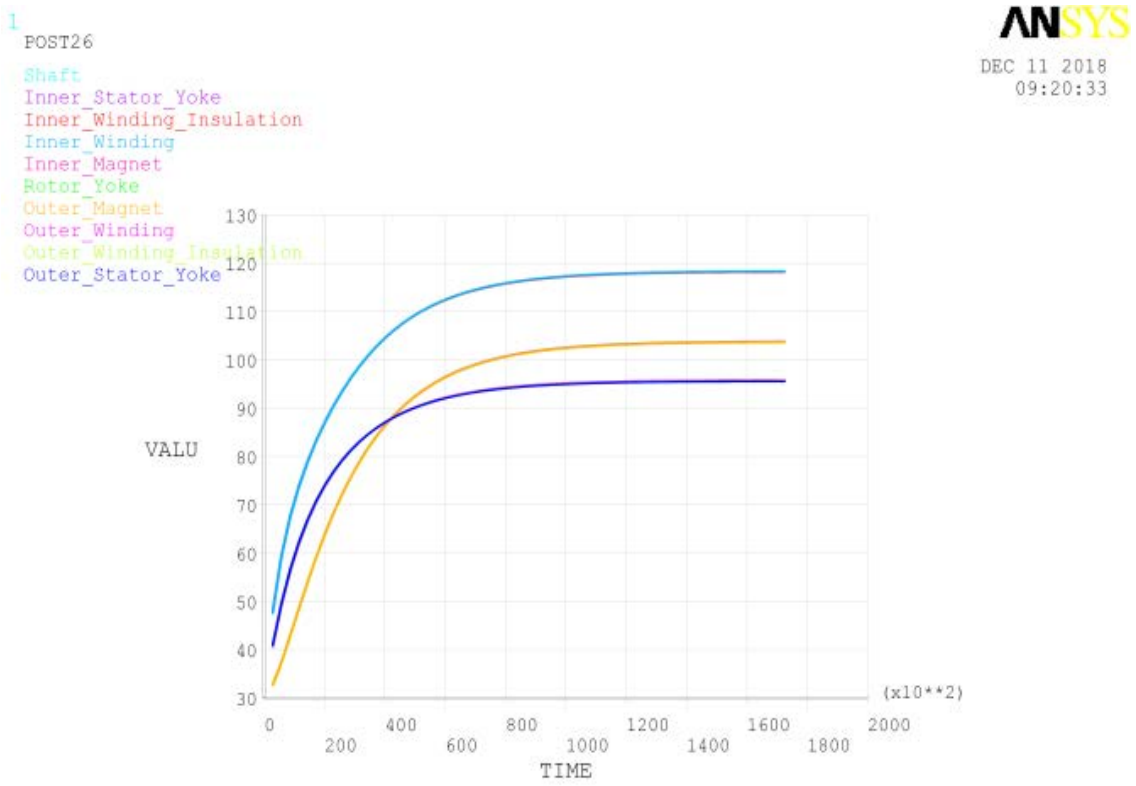

Fig. 5.19 Temperature variation in the different parts of model

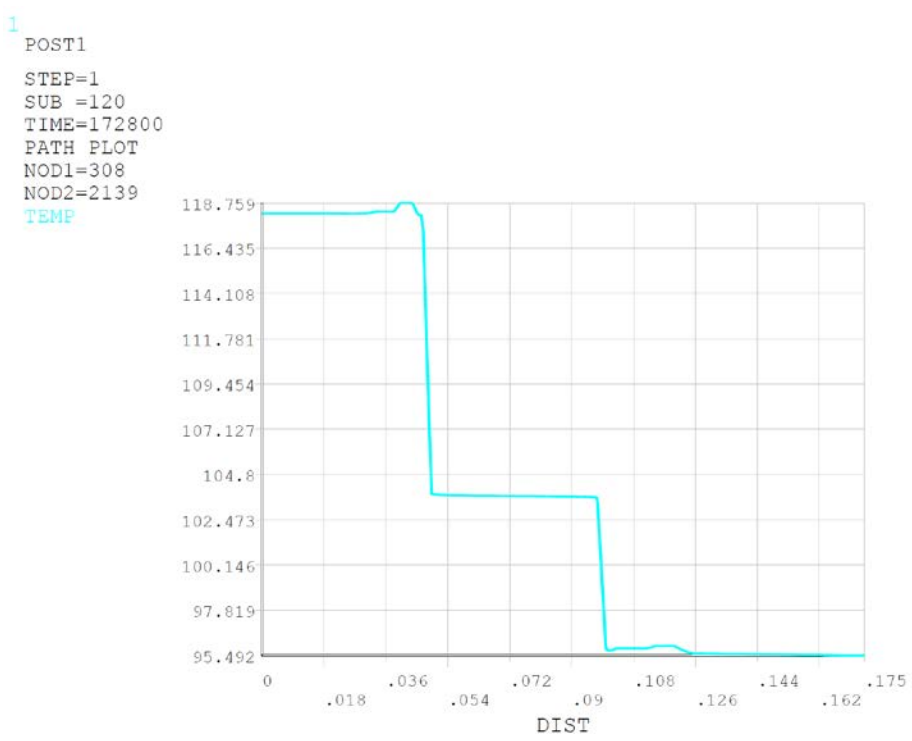

Fig. 5.20 Radial Temperature variation from inner to outer in model

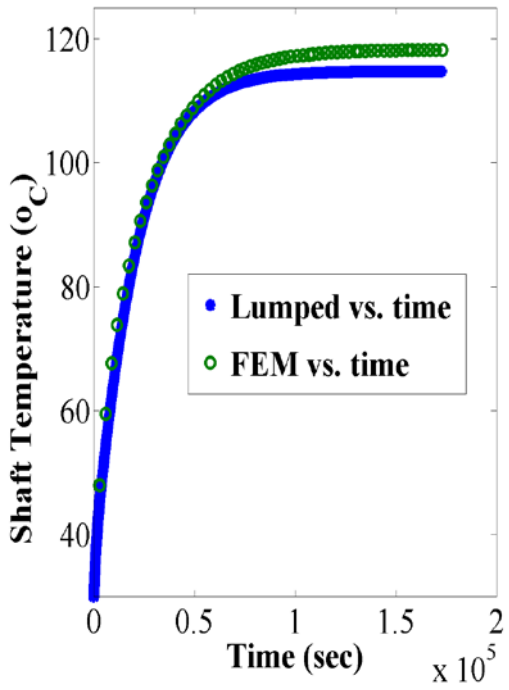

Fig. 5.21 Shaft temperature

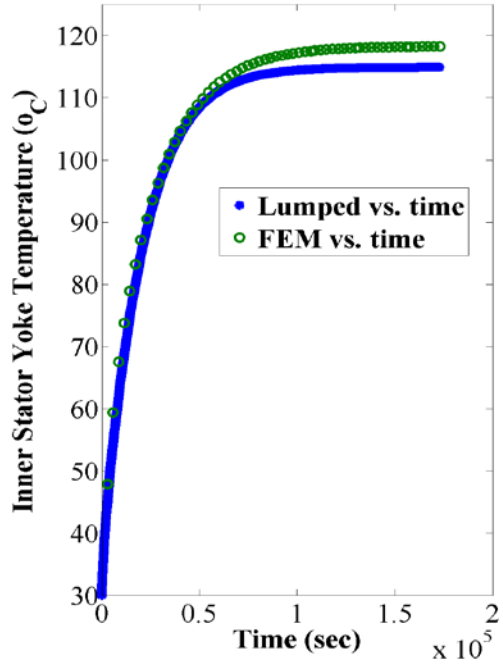

Fig. 5.22 Inner Stator Yoke temperature

Fig. 5.22 shows the temperature variation in the inner stator yoke using lumped parameter model method and the FEM. The steady state predicted temperature of the

inner stator yoke is 115.7ºC. The temperature is directly associated with the insulating material between the lamination of core. The thermal modelling helps for selecting the class of the thin layer of insulation placed between the laminations before the manufacturing of core. Table 2.3 lists the insulation materials for lamination and corresponding maximum operating temperature. The Class B insulating material is therefore appropriate for rotor yoke lamination.

Fig. 5.23 shows the temperature variation of inner stator winding using lumped parameter model method and FEM analysis. The error in steady state temperature using lumped parameter is found to be 2.26% higher than the FEM results. The predicted steady state temperature using lumped parameter model method is 115.7^{o}C which is lesser than FEM result. Appropriate winding insulation is mandatory to ensure safe operation of the generator. The list of copper winding insulating materials as mentioned in Table 2.1 suggests that the class E winding insulating material has low cost and is a reliable material for this purpose.

Fig. 5.24 shows the temperature variation of the inner permanent magnet using lumped parameter model method and FEM analysis. The error in steady state temperature using lumped parameter is found 3.23% lower than the FEM results. The predicted steady state temperature using lumped parameter model method is 107.23^{o}C, which is higher than the FEM result. Since PM are highly temperature sensitive so appropriate PM material is mandatory to ensure safe and reliable operation of the generator. The list of PM materials as mentioned in Table 2.6 suggests that the NdFeBH grade seems to be appropriate as the inner PM for the proposed DSFP-PMSG.

Fig. 5.25 shows that the temperature variation in the rotor yoke using lumped parameter model method and the FEM analysis. The error in steady state temperature using lumped parameter is found to be 2.31% lower than the FEM results.

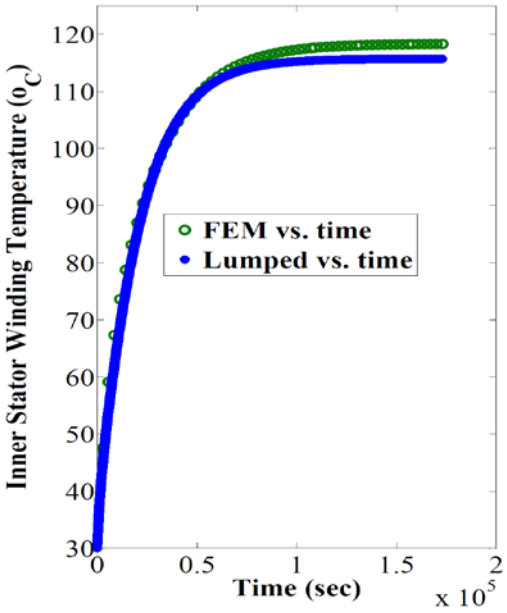

Fig. 5.23 Inner stator winding temperature

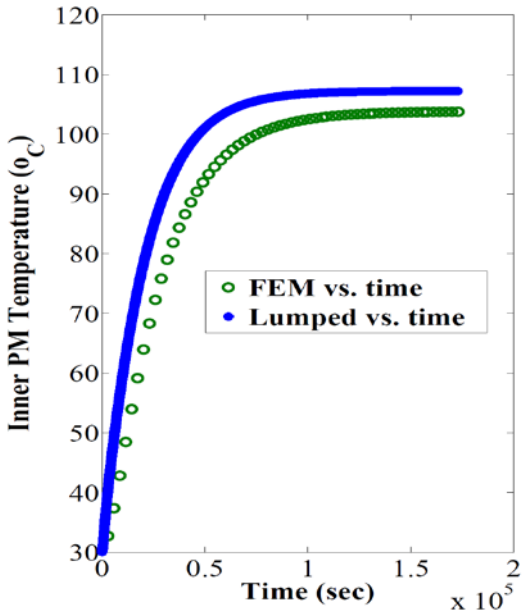

Fig. 5.24 Inner PM temperature

The predicted steady state temperature using lumped parameter model method is 106.13^{o}C which is found to be higher than FEM result. The temperature is directly associated with the insulating material between the lamination of rotor core. The thermal modelling helps in selecting the class of the thin layer of insulating material placed between the laminations before the manufacturing of the core. The different insulating materials for the insulating the laminations and corresponding maximum operating temperature are mentioned in Table 2.3. The Class B insulating material is therefore appropriate for rotor yoke lamination.

Fig.5.26 shows the temperature variation of the outer permanent magnet using lumped parameter model method and FEM analysis. The error in steady state temperature using lumped parameter is found to be 1.95% lower than the FEM results. The predicted steady state temperature using lumped parameter model method is

105.71°C, which is higher than FEM result. Since PM are highly temperature sensitive so appropriate PM material is mandatory to ensure safe and reliable operation of the generator. The list of PM materials as mentioned in Table 2.6 suggests that the NdFeBH seems to be appropriate as the outer PM for the proposed MCDSFP-PMSG.

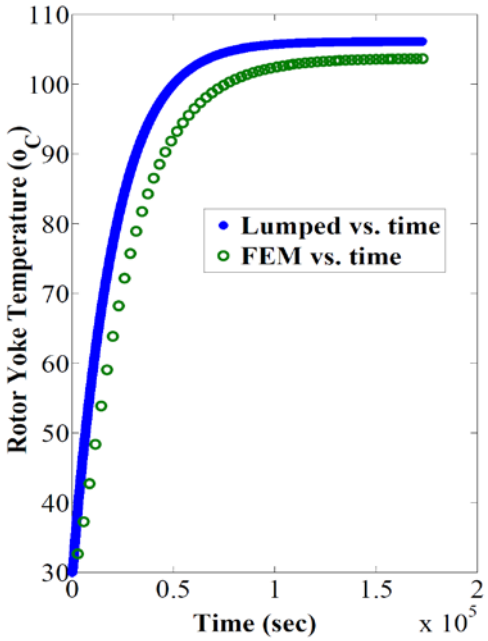

Fig. 5.25 Rotor Yoke temperature

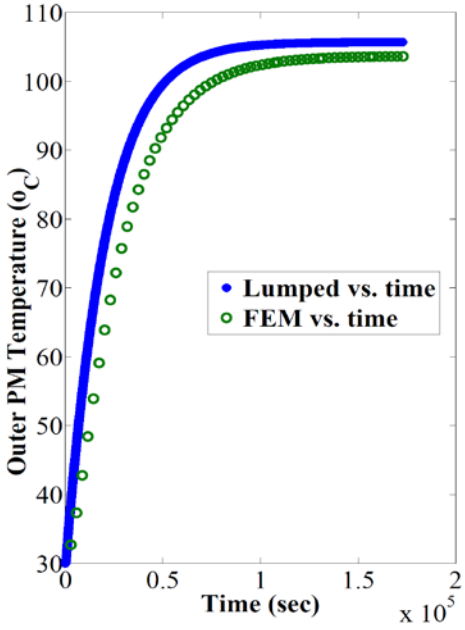

Fig. 5.26 Outer PM temperature

Fig.5.27 shows the temperature variation of outer stator winding using lumped parameter model method and FEM analysis. The error in steady state temperature using lumped parameter model is 3% lower than the FEM results. The predicted steady state temperature using lumped parameter model method is 98.74°C which is higher than FEM result. Appropriate winding insulation is mandatory to ensure safe operation of the generator. From the list of copper winding insulating materials as mentioned in Table 2.1 suggests that the class A winding insulating material has the lower cost and is a reliable material for this purpose.

Fig. 5.28 shows that the temperature variation in the inner stator yoke using lumped parameter model method and the FEM. The error in steady state temperature using lumped parameter is found to be 1.57% higher than the FEM results. The

predicted steady state temperature using lumped parameter model method is 94.06^{o}C which is lesser than FEM result. The temperature is directly associated with the insulating material between the lamination of core. The thermal modelling helps for selecting the class ofthe thin layer of insulation placed between the laminations before the manufacturing of core. Table 2.3 lists the insulation materials for lamination and corresponding maximum operating temperature. The Class B insulating material is therefore appropriate for outer stator yoke lamination.

The predicted temperature of the various sections namely shaft, inner stator yoke, inner stator winding, inner PM, rotor yoke, outer PM, outer stator winding and outer stator yoke of the proposed MCDSFP-PMSG using LPM and FEM are presented in Table 5.5. The percentage error of the predicted temperatures for different sections of generator is very less. This confirms good accuracy level of the Lumped parameter model for predicting the temperature distribution in the proposed MCDSFP-PMSG.

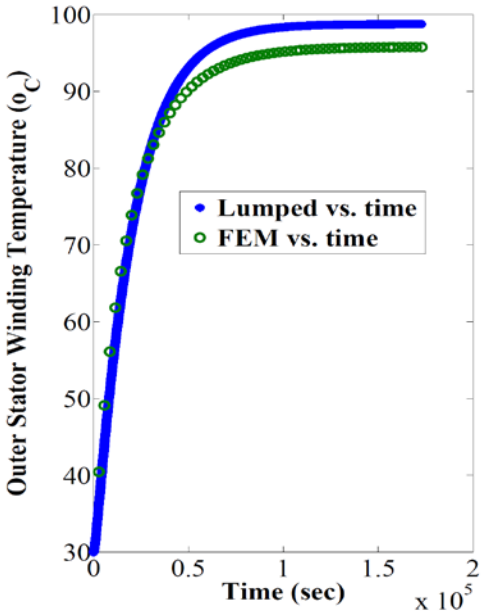

Fig. 5.27 Outer Stator Winding temperature

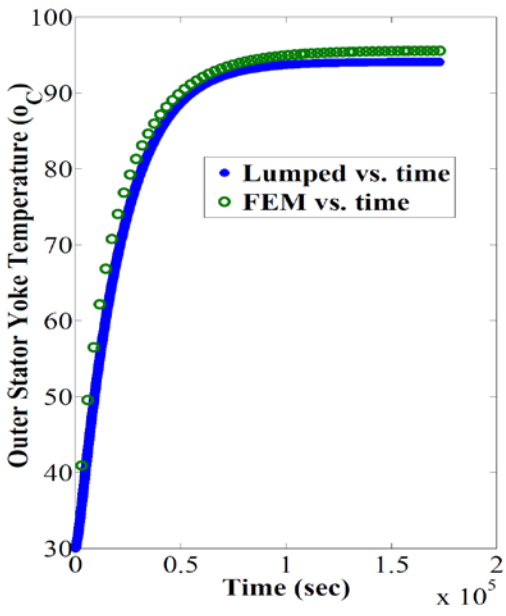

Fig. 5.28 Outer Stator Yoke temperature

Table 5.5 : Steady state temperature of different part of MCDSFP-PMSG

Parameter	Lumped (in ^{O}C)	FEM (in ^{O}C)	%Error
Shaft	114.764	118.221	3.012
Inner stator yoke	114.868	118.217	2.915
Inner stator winding	115.701	118.316	2.260
Inner PM	107.230	103.761	-3.235
Rotor yoke	106.136	103.682	-2.312
Outer PM	105.711	103.640	-1.959
Outer stator winding	98.7368	95.754	-3.020
Outer stator yoke	94.0673	95.549	1.575

5.3.4 Summary

The Section 5.3 deals with the thermal modelling for the MCDSFP-PMSG. The lumped parameter model method is used, which is simple and fast analytical technique for predicting the temperature distribution inside the proposed generator. Unlike the lumped parameter thermal model presented for SSFP-PMSG it also includes the axial direction heat flow and heat flow due to radiation. Due to which the accuracy of the temperature prediction enhances and the error is limited within the 3.3% with respect to the simulated FEM results. Based on the predicted temperature various materials are identified for the development and safe operation of the machine. This include class B insulating material for inner stator and rotor yoke whereas class A for outer stator laminations, class E insulating material for inner stator windings whereas class A for outer stator winding and NdFeB H grade material for both the inner and outer permanent magnets. Maintenance issues due to shaft temperature on bearing lubrication viscosity are also highlighted.

5.4 Conclusion

Section 5.2 and Section 5.3 deals the thermal modelling for the SSFP-PMSG and MCDSFP-PMSG respectively. The lumped parameter model has been used as analytical tool for fast prediction of the temperature distribution in the generator Moreover, the lumped parameter model used for MCDSFP-PMSG is more effective which also considers radiation effect as well as axial flow of heat loss. Axial flow enables more effectively the convection and radiation heat flow process from different parts of generator to the environment. Due to which the accuracy of the temperature prediction enhances and the error is limited within the 3.3% with respect to the simulated FEM results for the MCDSFP-PMSG.